



**HAL**  
open science

# High-temperature elastic softening of orthopyroxene and seismic properties of the lithospheric upper mantle

Bruno Reynard, Jay D. Bass, Jon Brenizer

## ► To cite this version:

Bruno Reynard, Jay D. Bass, Jon Brenizer. High-temperature elastic softening of orthopyroxene and seismic properties of the lithospheric upper mantle. *Geophysical Journal International*, 2010, 181 (1), pp.557-566. 10.1111/j.1365-246X.2010.04524.x . insu-00681715

**HAL Id: insu-00681715**

**<https://insu.hal.science/insu-00681715>**

Submitted on 5 Mar 2021

**HAL** is a multi-disciplinary open access archive for the deposit and dissemination of scientific research documents, whether they are published or not. The documents may come from teaching and research institutions in France or abroad, or from public or private research centers.

L'archive ouverte pluridisciplinaire **HAL**, est destinée au dépôt et à la diffusion de documents scientifiques de niveau recherche, publiés ou non, émanant des établissements d'enseignement et de recherche français ou étrangers, des laboratoires publics ou privés.

# High-temperature elastic softening of orthopyroxene and seismic properties of the lithospheric upper mantle

Bruno Reynard<sup>1</sup>, Jay D. Bass<sup>2</sup> and Jon Brenizer<sup>2</sup>

<sup>1</sup>Université de Lyon, Laboratoire de Science de la Terre, CNRS, Ecole Normale Supérieure de Lyon, 69007 Lyon, France. E-mail: bruno.reynard@ens-lyon.fr

<sup>2</sup>Department of Geology, University of Illinois, Urbana, IL 61801, USA

Accepted 2010 January 13. Received 2010 January 10; in original form 2009 September 30

## SUMMARY

Mineralogical models suggest that low velocity zones of the upper mantle may be accounted for by elasticity of dry rocks along geotherms away from the mid-oceanic ridges (MOR) while, closer to MOR, anelasticity plays a significant role in reducing shear wave velocities  $V_S$  and generating attenuation. We investigate the potential influence of elastic softening, precursor of high-temperature phase transition in orthopyroxenes, on the seismic properties of the upper mantle. *In situ* Brillouin and Raman spectroscopy were used to evidence pre-transitional behaviour at high temperature in natural San Carlos orthopyroxene. Pre-transitional behaviour induces a large softening of the acoustic and low frequency modes, resulting in a large anharmonic decrease of sound velocities, similar to that observed in the  $\text{MgSiO}_3$  end-member orthoenstatite. The high-temperature high-pressure phase diagram of enstatite is revised to account for the new phase transition, and a simple model is developed to evaluate elastic softening effects on the upper-mantle seismic properties, whose results depend much on the as yet poorly constrained pressure and compositional dependence of the phase transition boundary. Within the tested range of parameters, OPx softening is likely to affect the seismic properties of mantle rocks at depths shallower than 80 km in hot regions. Thus elastic softening of pyroxene is unlikely to affect the LVZ or continental lithospheric mantle unless the transition temperature is drastically reduced by incorporation of aluminium in orthopyroxene. It will contribute to a decrease of  $V_S$  near MOR, hot spots and evolved continental rifts, where it can explain part of the non-linear high-temperature decrease of  $V_S$  in the lithospheric oceanic mantle. It will affect the magnitude of anelastic effects and the nature of the likely mechanisms of attenuation required to match seismological observations.

**Key words:** Composition of the mantle; Elasticity and anelasticity; Phase transition; Seismic attenuation.

## 1 INTRODUCTION

Enstatites  $(\text{Mg,Fe})\text{SiO}_3$  are major mantle rock-forming minerals that undergo several phase transitions between various orthorhombic or monoclinic polymorphs over the pressure–temperature range of the upper mantle. These transitions affect the elastic properties of pyroxenes and the mineralogical interpretation of upper-mantle seismic properties. At high pressure, *Pbca* orthoenstatite (OEn) transforms to *C2/c* high-clinoenstatite (Pacalo & Gasparik 1990), a first-order transformation associated with large change of volume, vibrational and elastic properties (Angel *et al.* 1992; Ross & Reynard 1999; Kung *et al.* 2004). Protoenstatite (PEn, Atlas 1952) is a high-temperature phase of OEn with a *Pbcn* structure (Smith 1959; Smyth 1971), and a high-temperature clinoenstatite (HT-CEn, *C2/c*) is formed on heating of *P2<sub>1</sub>/c* low-clinoenstatite (LCEn) above 1200 K (Sharma 1989; Shimobayashi & Kitamura 1991). *In situ* X-ray diffraction studies confirm that the complex transformation schemes between LCEn–OEn–PEn are kinetically con-

trolled; hence the transitions are of first-order character (Brown *et al.* 1961; Sadanaga & Okamura 1969; Smyth 1974). High-temperature Brillouin measurements on nearly pure  $\text{MgSiO}_3$  demonstrated that OEn displays softening of sound velocities and elastic constants (Jackson *et al.* 2004a). Elastic softening is attributed to pre-transitional effects of a high-temperature second-order transition hidden by the first-order OEn–PEn transformation, and may have important consequences in the modelling and understanding of upper-mantle seismic properties especially in hot regions (Stixrude & Lithgow-Bertelloni 2005a; Afonso *et al.* 2008). Pre-transitional effects and phase transition have also been evidenced by Raman spectroscopy in  $\text{MgSiO}_3$  (Sharma 1989). To extend this study to mantle compositions, we have performed *in situ* Brillouin and Raman spectroscopy on San Carlos orthopyroxene. Although the presence of iron in the natural sample hinders the transition to PEn that occurs in end-member composition  $\text{MgSiO}_3$ , pre-transitional softening of elastic constants and low frequency Raman modes were observed. A simple model is proposed to extrapolate elastic

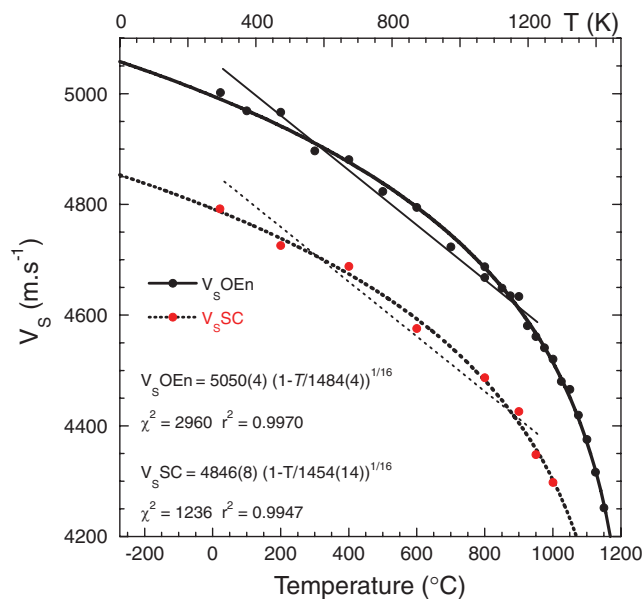


**Figure 1.** High-temperature shear velocities in San Carlos orthopyroxene (SC OPx; red circles) are compared with those of nearly pure  $\text{MgSiO}_3$  OEn (black circles) from Zabargad (Jackson *et al.* 2004a,b). Data were fitted to eq. (1). Fits with free  $n$  yields  $n = 15.8(5)$  with  $T_C = 1487(11)$  K, and  $n = 16.9(25)$  with  $T_C = 1430(63)$  K, for OEn and SC OPx, respectively. Fit parameters are poorly constrained for SC OPx, while they are better constrained from OEn data over a large temperature range. Thus we fixed  $n = 16$  for fitting both data sets, and obtained ‘critical’ temperatures  $T_C$  of 1484 and 1454 K for OEn (full curve) and SC OPx (dashed curve), respectively. Sublinear temperature dependences of  $V_S$  calculated in internally consistent thermodynamic data set (Stixrude and Lithgow-Bertelloni, 2005a) are approximated by the full (OEn) and dashed (SC OPx) lines.

softening to upper-mantle conditions and take it into account in shear wave velocity calculations for geophysical applications.

## 2 EXPERIMENTAL

For Raman spectroscopy, we used synthetic  $\text{MgSiO}_3$  OEn single-crystals (Thiéblot *et al.* 1999), natural pure enstatite ( $\text{Fs}_0$ ) from Zabargad (Jackson *et al.* 2004a), and natural San Carlos OEn single-crystals ( $\text{Fs}_{7-10}$ ), where Fs is the mol per cent of ferrosilite end-member. Crystals about 0.1 mm thick and 0.5 mm long were loaded in a Leitz 1350 heating stage attached to a DILOR<sup>TM</sup> LabRam HR 800 microspectrometer (see Okuno *et al.* 1999, for details). Peak position and width were fitted assuming Voigt profiles using Peakfit<sup>TM</sup> program. Resolution is about  $2 \text{ cm}^{-1}$  and reproducibility about  $1 \text{ cm}^{-1}$ . Brillouin spectroscopy was performed on single crystals of San Carlos OPx using the setup described by Bass (1989) and Jackson *et al.* (2004a). In brief, an Ar-ion laser ( $\lambda = 514.5 \text{ nm}$ ) was used for the incident light source, and a Sandercock-style tandem Fabry-Perot interferometer was used to analyse the scattered light. Brillouin spectra were collected with a  $90^\circ$  symmetric scattering geometry at ambient conditions, and at high temperatures. A small resistance heater (Sinogeikin *et al.* 2000) was used for high-temperature Brillouin measurements to  $>1273 \text{ K}$ . Brillouin spectra were recorded in several directions within the [100], [010]

and [001] crystallographic planes. This allowed solving for the nine single-crystal elastic moduli of this orthorhombic mineral at all temperatures. Further details will be given elsewhere (Brenizer & Bass, in preparation).

## 3 RESULTS

Sound velocities of SC OPx could be obtained up to about 1273 K, a temperature above which phase transformation under the laser occurred. Phase transformations are interpreted as feedback effects between oxidation of Fe and laser heating which becomes significant above 1273 K. Laser absorption on the measurement spot causes slight oxidation at high temperature, which in turn increases laser absorption and heating because black oxides are formed, eventually resulting in melting at the laser spot. Thus the temperature range for SC OPx elastic data is more restricted than for OEn (Jackson *et al.* 2004a; Fig. 1). Although all moduli were refined from measured  $P$ - and  $S$ -wave velocities, we report here the values for the aggregate shear velocities  $V_S$ , which is the pertinent property for modelling isotropic shear wave velocities in the mantle (Fig. 1, Table 1), using the Voigt–Reuss–Hill average scheme. As the Voigt and Reuss values differ by less than 2 per cent, the error introduced by the averaging scheme is  $\pm 1$  per cent.

Raman-peak frequency decreases and linewidth increases were observed up to 1473 K. Several Raman modes, especially the lowest lying peaks in the  $80\text{--}150 \text{ cm}^{-1}$  range at room temperature, show non-linear behaviour with temperature (Fig. 2; Table 2). Our results on pure enstatite are consistent with those of Sharma (1989). The increase of linewidths with temperature is also non-linear, especially above about 973 K. These observations are valid for both  $\text{MgSiO}_3$  end-member and San Carlos sample, although the data are of better quality for the end-member, yielding more precise refinements of peak position and width. This explains the larger scattering of data and impossibility to accurately follow the lowest frequency mode parameters above 1423 K in San Carlos sample (Fig. 2). In the 1473–1523 K range depending on the crystal and heating conditions, pure OEn undergoes a phase transition to PEn while the San Carlos oxidizes above 1473 K even though Ar- $\text{H}_2$  (2 per cent) gas is fluxed in the sample chamber. Laser heating or photochemical effects may promote oxidation as discussed above. Other Raman characteristics of the transformation have been described in details (Sharma 1989; Reynard *et al.* 2008; Zucker & Shim 2009).

## 4 HIGH-TEMPERATURE TRANSITION IN MANTLE ORTHOPYROXENES

### 4.1 Compositional dependence

The non-linear high-temperature behaviour of  $V_S$  in SC OPx parallels that of OEn, and is attributed to elastic softening precursor of a phase transition (Jackson *et al.* 2004b). The available data for SC OPx are relatively limited to 1273 K, while most of the softening occurs at higher temperature in OEn, with a decrease of the shear modulus being twice higher than that expected from harmonic sublinear extrapolation (Stixrude & Lithgow-Bertelloni 2005b) at 1423 K (Fig. 1). Raman spectroscopy provide further

**Table 1.** High temperature aggregate shear wave velocities of SC OPx from Brillouin measurements.

$T$ (K)	295	473	673	873	1073	1173	1223	1273
$V_S$ ( $\text{m s}^{-1}$ )	4792	4726	4688	4576	4487	4426	4348	4298

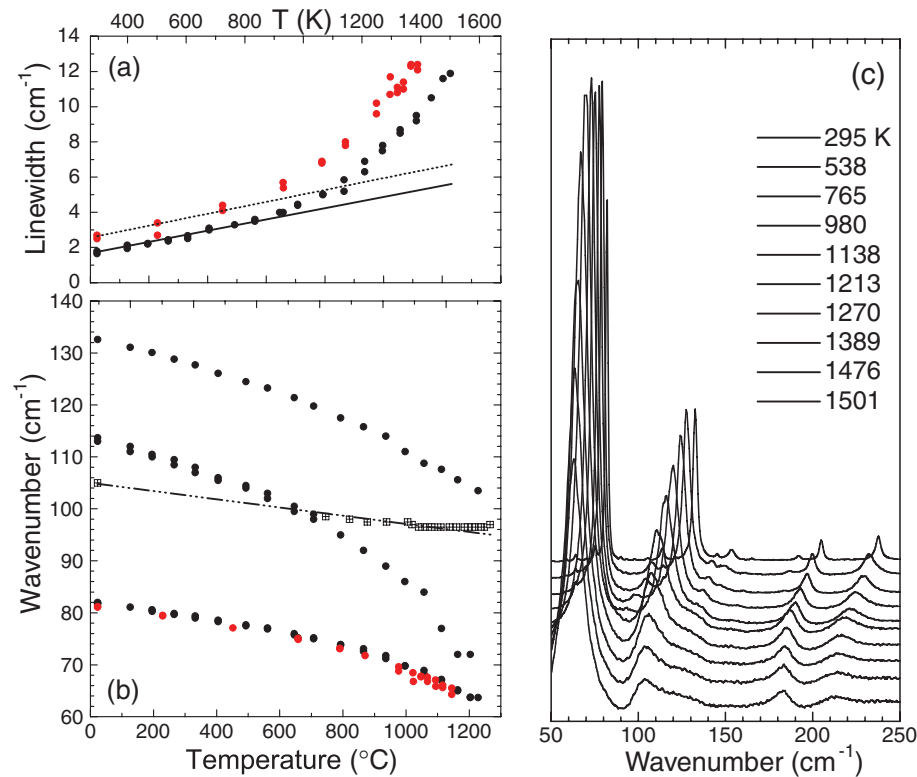


**Figure 2.** Temperature dependence of Raman active low-energy mode frequencies, and linewidth of the lowest frequency mode (*ca.* 80 cm<sup>-1</sup> at ambient conditions) in OEn and SC OPx. Corresponding spectra for OEn are shown on the right from 295 (top panel) to 1501 K. Note the temperature interval for displayed spectra is not constant. Black circles: MgSiO<sub>3</sub> OEn; red circles: SC OPx; open squares: PEn. Critical behaviour of the low frequency modes is illustrated by strong curvature of their temperature dependence and by non-linear increase of linewidth. In comparison, lowest frequency mode of PEn from metastably cooled and quenched samples has a linear temperature dependence (dash-dotted line). OEn and SC OPx lowest frequency modes show parallel evolution up to the highest temperatures of 1420 K for SC OPx, suggesting similar temperature dependence for elastic constants corresponding to closely related acoustic modes and justifying the use of similar fit parameters for shear velocities of OEn and SC OPx (Fig. 1).

evidence that the softening behaviour in SC OPx extends to temperatures higher than 1273 K because low-frequency modes have a non-linear temperature dependence (Fig. 2, Table 2). The lowest energy Raman-active modes are derived from Brillouin-zone (BZ) edge acoustic branches whose frequencies depend on the elastic constants and sound wave velocities. Their softening and the strong increase in linewidths is caused by strong anharmonic effects (Pine & Tannenwald 1969). Along with elastic softening, these effects are attributed to the onset of a displacive, possibly *Pbca* ↔ *Cmca*, transition (Jackson *et al.* 2004a) that does not go to completion in MgSiO<sub>3</sub> because of the occurrence of the first-order transition to PEn.

Pre-translational behaviour at high temperatures is a common observation in various orthopyroxenes. Thus the displacive *Pbca* ↔ *Cmca* transition postulated for pure OEn may well occur over a compositional range that covers that of mantle orthopyroxene, except for the effect of aluminium that has not been investigated thus far. Non-linear variations of volume, cell parameters and bond angles have been observed in orthopyroxenes on the En–Fs join, for compositions Fs<sub>25</sub> (transition above 1027 °C; (Yang & Ghose 1995), Fs<sub>100</sub> (transition at 1153 K, (Sueno *et al.* 1976; Sueno *et al.* 1984), Fs<sub>6</sub> orthopyroxene up to 1473 K, (Gatta *et al.* 2007), and in a 3 per cent Ca-bearing orthoenstatite, (Ohi *et al.* 2008). The exact nature of the phase transition may vary from OEn to PEn in MgSiO<sub>3</sub> (Smyth 1971), while ferrosilite transforms to a high-temperature C2/c form distinct from the high-pressure isostructural form (Sueno

*et al.* 1984), and an isostructural *Pbca*–*Pbca* transition is reported in Ca-bearing enstatite (Ohi *et al.* 2008). Compositional dependence of transition temperatures is difficult to evaluate precisely because the nature of the transition may vary with composition, but increasing Fe content seems to slightly decrease the temperature at which pre-translational effects occur (Yang & Ghose 1995).

#### 4.2 Phase diagram of MgSiO<sub>3</sub> and Clapeyron slope of the high-temperature transition

Taking into account the high-temperature phase transition in MgSiO<sub>3</sub>, re-appraisal of petrological experimental determinations of the phase diagram allows constraining the Clapeyron slope of the displacive *Pbca* ↔ *Cmca* transition for pure OEn. Taken at face value the brackets on the OEn ↔ PEn transition at ambient (1258 ± 10 K; Atlas, 1952) and high-pressure conditions (Anastasiou & Seifert 1972; Boyd *et al.* 1964; Chen & Presnall 1975; Kushiro *et al.* 1968) define a peculiar phase boundary between PEn and OEn. A first segment with Clapeyron slope of about 400 K GPa<sup>-1</sup> up to 1673 K is followed by a slightly negative Clapeyron slope segment. Chen & Presnall (1975) gave a kinetic interpretation of this observation whereby the impossibility of quenching PEn or its back-transformation product LCEn when temperatures exceed 1673 K causes an ‘erroneous’ attribution of data points to the OEn stability field (Fig. 3a). In light of the Brillouin results and interpretation by Jackson *et al.* (2004a) of a hidden displacive transition

**Table 2.** Ambient temperature Raman mode frequencies ( $\nu$ ) and temperature dependences ( $\partial\nu/\partial T$ ) for the orthorhombic (*Pbca*, OEn) and high-temperature (*Cmca*?, HTEn) MgSiO<sub>3</sub> enstatite polymorphs.

HTEn		OEn		$\partial^2\nu/\partial T^2$ ( $\times 10^5$ ) (cm <sup>-2</sup> K <sup>-2</sup> )
$\nu$ (cm <sup>-1</sup> )	$\partial\nu/\partial T$ (cm <sup>-1</sup> K <sup>-1</sup> )	$\nu$ (cm <sup>-1</sup> )	$\partial\nu/\partial T$ (cm <sup>-1</sup> K <sup>-1</sup> )	
105	-0.006(1)	82	-0.002(2)	-1.03(13)
115		105		
118		114	-0.010(3)	-1.7(3)
131		133	-0.011(1)	-1.0(1)
138		145	-0.007(1)	-0.7(1)
141		153	-0.014(1)	
156		160		
177		167	-0.0126(5)	
188	-0.0154(10)	193	-0.017(1)	
193		196	-0.004(1)	
210		205	-0.0189(5)	
213	-0.0128(7)	224		
		235		
		237		
241		240	-0.021(1)	
251		244		
258		259	-0.014(2)	
271	-0.010(1)	276	-0.013(2)	-0.6(2)
274		283		
286		295		
299		301	-0.014(1)	
305		308		
		313		
		323		
331	-0.0191(7)	331		
342		342	-0.0261(6)	
371		360		
375		378		
384		383	-0.019(2)	
403		400	-0.023(1)	
412		416		
420		421	-0.015(2)	-0.8(2)
430		444	-0.020(1)	
441		457		
466		471	-0.017(1)	
478		486		
513		519		
525		525	-0.012(2)	
		539	-0.013(2)	
		546		
548	-0.008(2)	551	-0.015(2)	
569		579		
581		594		
673	-0.0159(5)	663	-0.0115(16)	-0.26(16)
		685	-0.0168(11)	-0.32(8)
729				
752		750		
848		851	0.00(1)	
856		885	-0.006(3)	
896		892		
925		928		
939		935	-0.023(3)	
		989		
1013	-0.023(1)	1012	-0.0179(10)	-0.29(8)
1028	-0.027(2)	1033	-0.0186(24)	-0.58(19)
1037	-0.029(15)	1038		
		1061		

at a higher temperature than the OEn-PEn transition, an alternative explanation is proposed (Fig. 3b). Three different phase boundaries originate from a triple point near 0.85 GPa and 1673 K. The first boundary is the OEn-PEn transition with Clapeyron slope of about

400 K GPa<sup>-1</sup>, the nearly constant-pressure segment at high temperatures the transition between PEn and the postulated, possibly *Cmca*, high temperature phase, and the third segment the stable extension of the ambient pressure metastable displacive transition from OEn

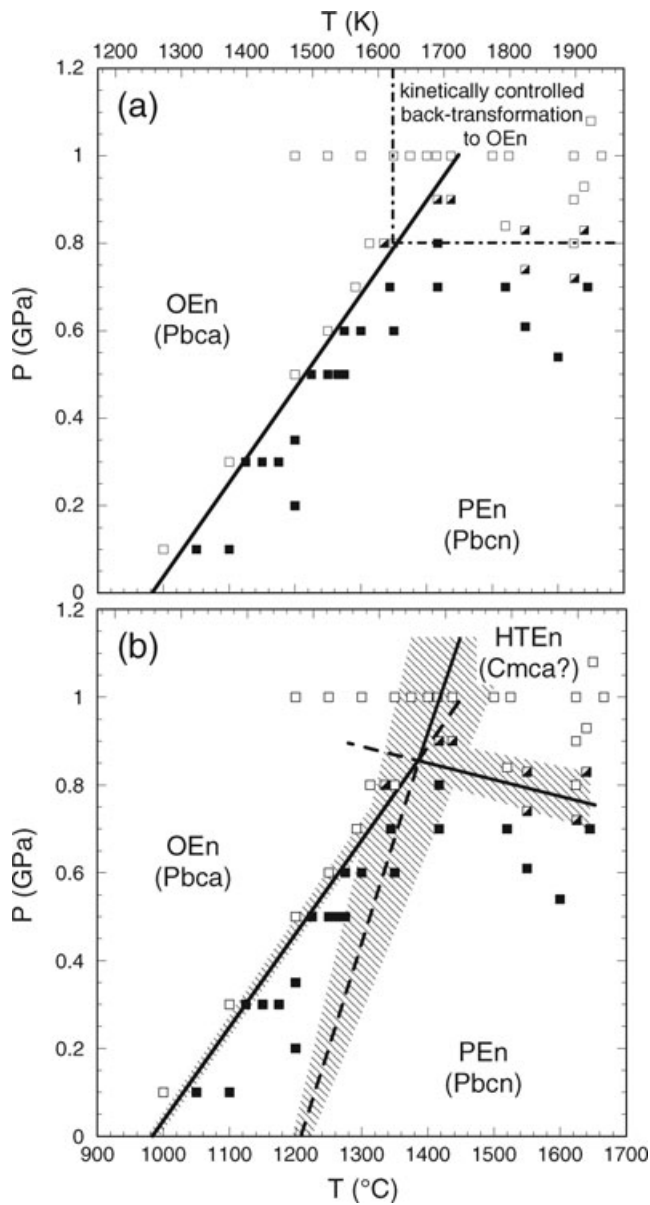


**Figure 3.** High-pressure high-temperature phase diagram of  $\text{MgSiO}_3$  enstatite showing experimental quench products as open squares for OEn, filled squares for assemblages interpreted as PEn, and half-filled squares for ambiguous assemblages. Boundary between OEn and PEn quench products shows a strong curvature near 1673 K and 0.8 GPa. This was interpreted (Chen and Presnall, 1975) as a single phase boundary between the stability fields of OEn and PEn with Clapeyron slope of  $400 \text{ K GPa}^{-1}$  where, when the transition is crossed above about 1733 K on quenching from the highest pressure–temperature points, only OEn can be quenched (a). We propose a new interpretation (b) with three stable phases, the HTEn form being quenched as OEn because of the reversible character of the OEn-HTEn (possibly  $Pbca \leftrightarrow Cmca$ ) displacive transition (Jackson *et al.* 2004a,b). Ambient pressure transition temperature is estimated from  $T_C$  in Fig. 1. Estimated Clapeyron slope for the OEn-HTEn transition is in the range  $100\text{--}300 \text{ K GPa}^{-1}$ , with most likely value around  $200 \text{ K GPa}^{-1}$ .

to the high-temperature phase. Only OEn can be quenched above the triple point because of the displacive nature of the phase transition on this third segment. Clapeyron slope of the displacive transition can be estimated from the location of the triple point and the ambient pressure transition temperature as  $210 \pm 90 \text{ K GPa}^{-1}$ .

## 5 MODELLING OF PRE-TRANSITIONAL ELASTIC EFFECTS IN MANTLE PYROXENE

The non-linear variations are observed in the high-temperature Brillouin and Raman data of the SC OPx and of OEn, and on cell parameters for various compositions. Thus these pre-transitional effects should be observed in compositions relevant to the Earth's mantle and be associated with lower velocities in hot zones of the upper mantle. To test that possibility, we develop here a simple model to take into account non-linear softening of sound velocities at upper-mantle pressures and temperatures. Because tomographic images and most seismic profiles are obtained for shear velocities, we focus on modelling  $V_S$  near the transition temperature and comparing our results to those from the thermodynamic data set of Stixrude & Lithgow-Bertelloni (2005b).

A Landau theory formalism can be used to qualitatively describe the changes in elastic constants with temperature for the proposed phase transition (Jackson *et al.* 2004a, b). This approach gives self-consistent expressions for the free enthalpy and elastic constants but they contain too many parameters to be constrained by the available data. Thus we chose to use a simpler formalism to fit the data, which uses the typical term  $(1 - T/T_C)^{1/n}$  that is present in Landau-type expansions of the free enthalpy and various properties as a function of temperature:

$$V_S(T) = V_S(T_r) \left(1 - \frac{T}{T_C}\right)^{\frac{1}{n}}. \quad (1)$$

Expression (1) has the character of being sublinear at low temperatures, and reproduces the strong curvature of the shear wave velocity data near  $T_C$  with only three adjustable parameters, the shear velocity  $V_S(T_r)$  at reference temperature  $T_r$ , the characteristic temperature  $T_C$  and exponent  $n$  of the transition (Fig. 1). We obtain  $n = 15.8(5)$  and  $T_C = 1487(11) \text{ K}$ , and  $n = 16.9(25)$  and  $T_C = 1430(63) \text{ K}$  for OEn and SC OPx, respectively. Because data for SC OPx are limited to 1273 K, we preferred to fit both data sets with  $n$  fixed to a value of 16, and obtained  $T_C$  of 1484(4) and 1454(14) K for OEn and SC OPx, respectively (Fig. 1).  $T_C$  is the temperature at which the fit with expression (1) for shear velocity or any variable (elastic modulus or Raman frequency) goes to a value of 0. Because of the simple equation used here,  $T_C$  and  $n$  are not equivalent to the critical temperature and order of the transition as defined in Landau theory (Carpenter & Salje 1998), although they are related to it. For the assumed  $Pbca \leftrightarrow Cmca$  phase transition in orthopyroxene, Landau theory predicts that some elastic moduli like  $C_{33}$  go to 0 at the transition temperature, while others like  $C_{55}$  decrease non-linearly close to  $T_C$  before reaching the value of the equivalent modulus in the high-temperature phase. Using expression (1),  $T_C$  will correspond to the 'true' transition temperature of 1462(12) K obtained from fit to data for  $C_{33}$  in OEn (Jackson *et al.* 2004a, b) while it is higher [1581(21) K] for  $C_{55}$ . The value obtained for  $V_S$ , which is a function of several  $C_{ij}$ , is only slightly higher than the actual transition temperature obtained from fitting  $C_{33}$ . Finally, it is unlikely that the softening observed here includes some attenuation effects given the high frequencies of the Brillouin measurement. Dispersion effects associated with the transition might affect  $V_S$  at seismic frequencies but cannot be estimated from the present data set.

In Raman spectroscopy, the OEn phase could be maintained up to measured temperatures of 1501 K before transition to PEn occurred, possibly triggered by the displacive transition. It is also maintained to similar temperature in some Brillouin runs. Differences of

3 per cent in the transition temperature among different runs in different experimental setups are within the uncertainties associated with temperature calibration and small temperature gradients in the cells. Thus the metastable transition temperature is estimated as  $1485 \pm 25$  K at ambient pressure, more than 200 K higher than the bracket of the stable OEn-PEn transition at  $1258 \pm 10$  K (Atlas 1952).

Fit with expression (1) is compared with sublinear expression from self-consistent thermodynamic data set in the quasi-harmonic approximation (Stixrude & Lithgow-Bertelloni 2005b) in Fig. 1. We note that with the sublinear temperature dependence used by Stixrude & Lithgow-Bertelloni (2005b),  $V_S$  can be consistent within  $40 \text{ m s}^{-1}$  with that from expression (1) up to about 1200 K (Fig. 1), which is roughly the temperature interval of the data that were available to fit their model, if temperature derivatives near 873 K are matched and the initial value at 298 K is set to a slightly lower for expression (1) than for sublinear variations. In the absence of elastic data at both high pressure and temperature, we allowed the parameter  $n$  to vary with pressure so that  $V_S$  for orthopyroxene matches as closely as possible the values from Stixrude & Lithgow-Bertelloni (2005b) up to 1200 K while keeping adequate expression to describe the anharmonic deviation from linear temperature dependence of  $V_S$  due to the phase transition near  $T_C$  (see the Appendix). Allowing  $n$  to vary with pressure is justified in view of the observed change in character of displacive transitions (Carpenter & Salje 1998). The transition temperature at high pressure can be estimated from the proposed phase diagram (3) by simply extrapolating the ambient pressure value ( $1485 \pm 25$  K) to that at the triple point near 0.85 GPa ( $1673 \pm 50$  K), yielding a Clapeyron slope  $dT_C/dP = 210 \pm 90 \text{ K GPa}^{-1}$ . Deviations between the present expression and Stixrude & Lithgow-Bertelloni (2005b) model decrease with pressure as expected from the increase of  $T_C$  with pressure. At 10 GPa, results from both models agree within less than  $50 \text{ m s}^{-1}$  over the entire temperature range for the mantle because anharmonic effects vanished (Fig. 4). Thus significant effects of the transition on orthopyroxene shear velocities are restricted to shallow depths and high temperature regions of the mantle.

## 6 IMPLICATIONS FOR SEISMIC VELOCITIES AND ATTENUATION IN THE UPPER MANTLE

We corrected the polynomial expression for  $V_S$  in the upper mantle (Stixrude & Lithgow-Bertelloni 2005a) to account for the pre-transitional effects in mantle OPx near  $T_C$ :

$$V_S(T, P) = 4770 + 38P - 0.378T + X_{OPx} \Delta V_S(T, P), \quad (2)$$

where  $X_{OPx}$  is the mole fraction of OPx from thermodynamic modelling (Stixrude & Lithgow-Bertelloni 2005a),  $\Delta V_S(T, P)$  is the difference in shear wave velocity for OPx in the quasi-harmonic approximation (Stixrude & Lithgow-Bertelloni 2005b) and the present anharmonic model (see the Appendix). We neglected the effects that anharmonic changes in other thermodynamic properties of OPx near  $T_C$  might have on  $X_{OPx}$ . Instead we performed calculations assuming either  $X_{OPx}$  for 100 Ma or adiabatic geotherm (Fig. 5). Oceanic mantle temperatures were calculated using a 1-D half-space cooling model (Jaupart *et al.* 2007) as  $\theta = (1327 + 0.503z) \times \text{erf}[z/(2\sqrt{23\tau})]$ , where  $\theta$  is the temperature in  $^{\circ}\text{C}$ ,  $z$  the depth in km, and  $\tau$  the age in Ma. Effects on seismic profiles are compared with available lateral seismological models for the Pacific Ocean (Nishimura and Forsyth 1989; Maggi *et al.* 2006a; Priestley & McKenzie 2006; Weeraratne *et al.* 2007).

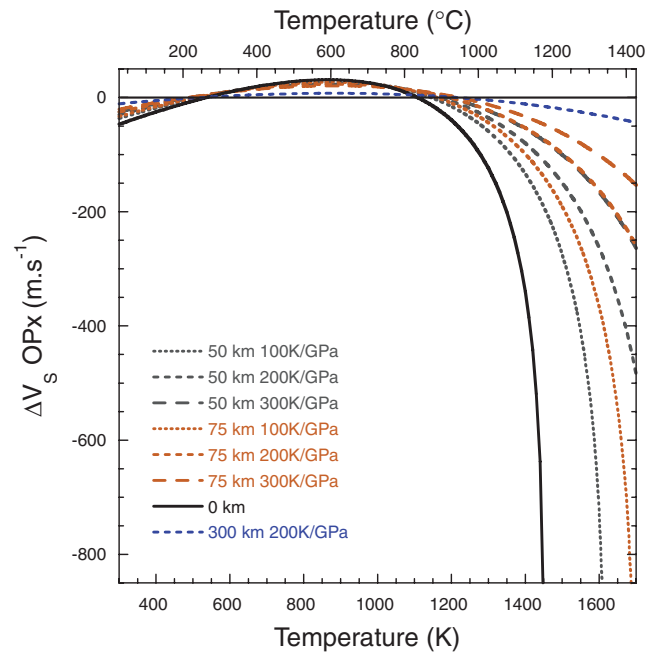


**Figure 4.** Difference between  $V_S$  of orthopyroxene from the present anharmonic softening model and the self-consistent quasi-harmonic model (Stixrude and Lithgow-Bertelloni, 2005b) as a function of temperature for three depths of 50, 75 and 300 km, and three Clapeyron slopes of the transition of 100, 200 and 300  $\text{K GPa}^{-1}$ . Below about 1200 K, the difference is less than  $50 \text{ m s}^{-1}$  for pressures corresponding to depths up to 75 km. Above that temperature, elastic softening induces large differences that strongly decrease with increasing depth. At a pressure of 10 GPa corresponding to about 300 km depth, the difference is less than  $20 \text{ m s}^{-1}$  up to 1500 K whatever the Clapeyron slope, and less than  $50 \text{ m s}^{-1}$  at 1700 K because the elastic softening has vanished.

Comparison of lateral profiles at 50 and 75 km depths (Fig. 5a) shows that the correction introduced by the OPx transition can be quite high near the mid-oceanic ridges (MOR). Corrections with Clapeyron slope of  $100 \text{ K GPa}^{-1}$  are obviously inconsistent with the seismological data because they are higher than the  $V_S$  decrease associated with melting near MOR at 50 km depth, and lower at 75 km depth. Corrections for the preferred value of  $200 \text{ K GPa}^{-1}$  and highest values ( $300 \text{ K GPa}^{-1}$ ) are not very different and may be considered as maximum effects of the softening. Both account partly for the slight curvature of the  $V_S$  temperature relationship in the seismic data prior to the sudden drop induced by melting at MOR. It is worth noting that for the two latter values of the Clapeyron slope, the elastic softening never exceeds that observed by Brillouin spectroscopy at high temperature (i.e. about 30 per cent decrease of  $V_{SOPx}$ ). Vertical profiles (Fig. 5b) calculated for Clapeyron slope of  $200 \text{ K GPa}^{-1}$  and  $X_{OPx}$  extreme values for 100 Ma and adiabatic geotherms (Stixrude & Lithgow-Bertelloni 2005a) show that elastic softening of OPx has a significant effect for depths shallower than 80 km that correspond to the lithospheric mantle as defined from seismic anisotropy (Nishimura & Forsyth 1989; Maggi *et al.* 2006b; Nettles & Dziewonski 2008) or from sharp lithosphere–asthenosphere boundary (Kawakatsu *et al.* 2009; Rychert & Shearer 2009). Therefore it will not affect significantly the low velocity zone or continental lithospheric mantle, unless the incorporation of aluminium in OPx at high pressures reduces the transition temperature by a few hundred degrees. They do not exceed one third of the observed  $V_S$  anomaly at about 50 km

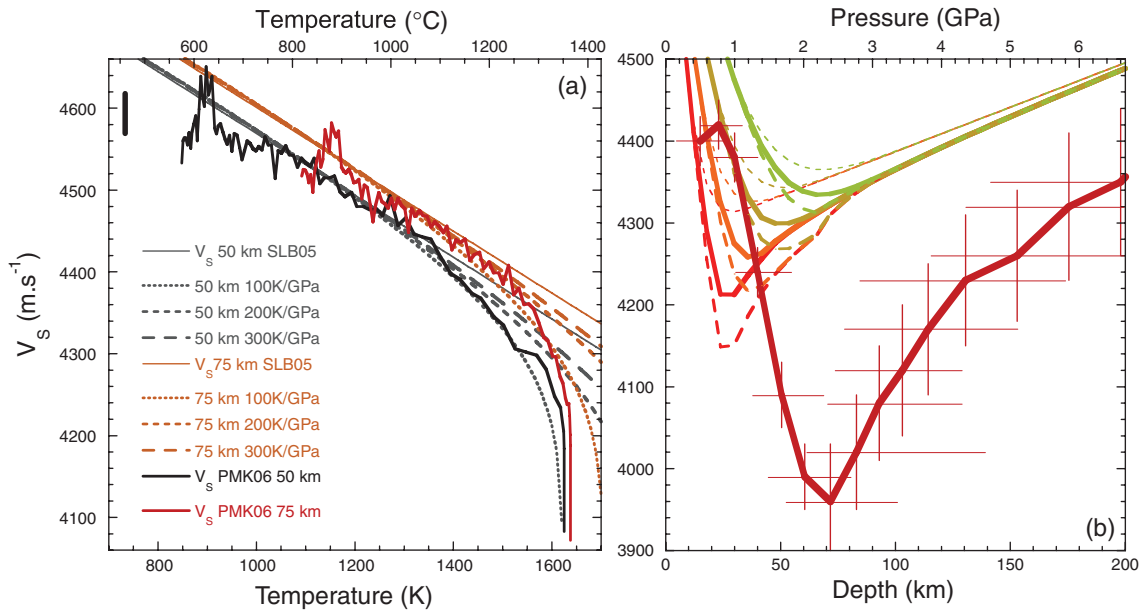


**Figure 5.** (a) Oceanic upper-mantle shear wave velocities as a function of temperature at depths of 50 and 75 km for a tomographic model of the oceanic lithosphere from Priestley and McKenzie (2006, PMK06) are compared with curves from harmonic mineralogical models (solid lines, Stixrude and Lithgow-Bertelloni, 2005a, SLB05) and models corrected for elastic softening of OPx with Clapeyron slopes of 100 (short dashed), 200 (medium dashed) and 300 K GPa<sup>-1</sup> (long dashed). Thick vertical black line shows uncertainties in observed  $V_S$ . Elastic softening of OPx accounts for part of the non-linear decrease of  $V_S$  above 1300 K prior to sharp decrease associated with partial melting at ridges above temperatures around 1625 and 1640 K at 50 and 75 km, respectively. (b) Vertical profiles of shear wave velocities in red, orange, yellow and green for 2.5, 5, 10 and 20 Ma oceanic geotherms, respectively. Thin dashed lines show profiles computed for harmonic high temperature behaviour of OPx elastic constants (Stixrude and Lithgow-Bertelloni, 2005a). Profiles calculated using modified expressions to account for elastic softening of OPx with preferred Clapeyron slope of 200 K GPa<sup>-1</sup> are shown as bold lines assuming two mole fractions of orthopyroxene  $X_{OPx}$ , a minimum one for a 100 Ma geotherm (full curves) and a maximum one  $X_{OPx}$  (dashed curves) along the adiabatic geotherm (Stixrude and Lithgow-Bertelloni, 2005a). They are compared with the observed shear wave velocity profiles (thick dark red curve) from the near mid-ocean ridge (MOR) GLIMPSE experiment (Weeraratne *et al.*, 2007). Predicted  $V_S$  reduction due to OPx softening is limited to the lithospheric mantle near MOR where it is at maximum one third of the observed minimum in  $V_S$  at MOR. This effect may slightly reduce the amount of partial melting or attenuation required to explain the shallow LVZ beneath MOR.

depth near the East Pacific Rise (Weeraratne *et al.* 2007), and can contribute to up to 20–35 per cent of the observed  $V_S$  decrease near MOR in the 10–50 km depth interval (Forsyth *et al.* 1998), thereby slightly reducing the amount of melt required to account for seismic observations.

A curvature of the  $V_S$  temperature dependence in the lithospheric oceanic mantle (Fig. 5a) observed before the sudden drop of velocity due to melting at MOR is usually attributed to anelastic effects on  $V_S$  (Afonso *et al.* 2008; Priestley & McKenzie 2006) that are not taken into account in the elastic mineralogical models. Attenuation effects can be introduced in the form (Minster & Anderson 1981):

$$V_S(\omega, T, P) = V_{S,0}(T, P) \left[ 1 - \frac{1}{2} \cot\left(\frac{\pi\alpha}{2}\right) Q^{-1}(\omega, T, P) \right], \quad (3)$$

where  $V_{S,0}(T, P)$  is the elastic shear wave velocity at null frequency that can be obtained from the models discussed so far,  $\omega$  is the shear wave frequency,  $\alpha$  is an exponent that varies typically from 0.1 to 0.3 and the quality factor  $Q$  depends on thermally activated processes (Karato & Jung 1998):

$$Q(\omega, T, P) = Q_0(\omega) \left[ \omega \exp\left(\frac{E + PV}{RT}\right) \right]^\alpha, \quad (4)$$

where  $E$  and  $V$  are the activation energy and volume, respectively. Further dependence on grain size or other parameters can be introduced depending on the mechanisms considered to cause attenuation (Faul *et al.* 2004; Jackson *et al.* 2002). Anelastic effects in

eq. (3) are the difference between the elastic models and seismological model (Fig. 5a), which is significantly affected by the elastic softening of OPx at 50 and 75 km depths. Therefore, we used this difference to evaluate an apparent quality factor  $Q^*$  from eq. (3). This is similar to the approach used by Priestley & McKenzie (2006), except that the elastic velocity and its temperature dependence is not fitted to seismological results at low temperatures but obtained from mineralogical modelling. Differences between  $V_S$  from mineralogical and seismological models become rapidly negligible when  $T$  decreases and corresponding errors on  $Q^*$  are high. Thus results are plotted only in a limited temperature range (1540–1640 K; Fig. 6) where the  $V_S$  difference between model and observations is significant (Fig. 5a). At lower  $T$ ,  $Q^*$  values level off to high average values above a few hundreds to more than one thousand depending on the model and  $\alpha$ . Higher apparent quality factors are obtained for the present  $V_S$  model accounting for elastic softening of OPx than for the linear harmonic model (Stixrude & Lithgow-Bertelloni 2005a). Two regimes are observed, one where  $\log Q^*$  depends linearly on inverse temperature, as expected from (4), and one where apparent  $Q^*$  drops rapidly at the highest  $T$ . This second regime corresponds to the MOR region where significant melt fractions directly affect the shear velocity and where relation (3) is no more valid to determine the  $Q^*$  values. Comparison with accurate regional determinations of  $Q$  near MOR (Yang *et al.* 2007) shows that  $\alpha$  exponent value of 0.1 is more likely than 0.3 in the 17–67 s range, but  $Q^*$  factors from both elastic models with and without elastic softening of OPx are

**Table 3.** Parameters of Arrhenius fit to eq. (3) for apparent quality factor  $Q^*$  ( $n$  is the number of data).

T range (K) <sup>a</sup>	log $Q_0$	$E$ (kJ mol <sup>-1</sup> )	T range (K) <sup>b</sup>	log $Q_0$	$E$ (kJ mol <sup>-1</sup> )	$n$
1637–1602	–14.5(9)	505(97)	1616–1592	–22.0(11)	729(155)	8
	<i>–10.6(7)</i>	<i>379(63)</i>		<i>–16.5(9)</i>	<i>556(95)</i>	
1637–1573	–14.4(7)	501(64)	1616–1570	–21.1(9)	701(97)	11
	<i>–10.0(6)</i>	<i>362(36)</i>		<i>–15.0(7)</i>	<i>508(52)</i>	
1637–1543	–14.2(6)	496(56)	1616–1542	–19.9(8)	664(79)	14
	<i>–9.4(5)</i>	<i>343(26)</i>		<i>–13.1(6)</i>	<i>450(34)</i>	

Note: Numbers in italics are those for  $Q^*$  estimated using linear temperature dependence of  $V_S$ .

<sup>a</sup>Temperature from equation in text.

<sup>b</sup>Temperatures from Priestley and McKenzie (2006).

consistent with the observations (Fig. 6). The  $\alpha$  exponent value of 0.1 is at variance of global observations in the same frequency range (Lekic *et al.* 2009) yielding 0.3. This difference may arise from scattering by small-scale heterogeneities that affect global models (Yang *et al.* 2007) and from the lack of sensitivity of global models at 50–200 km depths (Lekic *et al.* 2009). The linear portions of the log $Q^*$  versus  $1/T$  relationship at 75 km depth were fitted using eq. (3) assuming a fixed seismological frequency  $\alpha$ , neglecting the  $PV$  term, and for two models of lithospheric cooling (Jaupart *et al.* 2007; Priestley & McKenzie 2006). Fits could not be performed on the 50-km depth data because of the limited number of significant  $Q^*$  estimates but the similar slopes at 50 and 75 km depths indicate similar activation energies. Data were weighted to account for individual uncertainties on seismological  $V_S$  and assuming a constant uncertainty of 50 m s<sup>-1</sup> for the model values. Results from fits on different  $T$  intervals (Table 3) show that the final parameters depend little on the interval chosen, thus on the quality of apparent

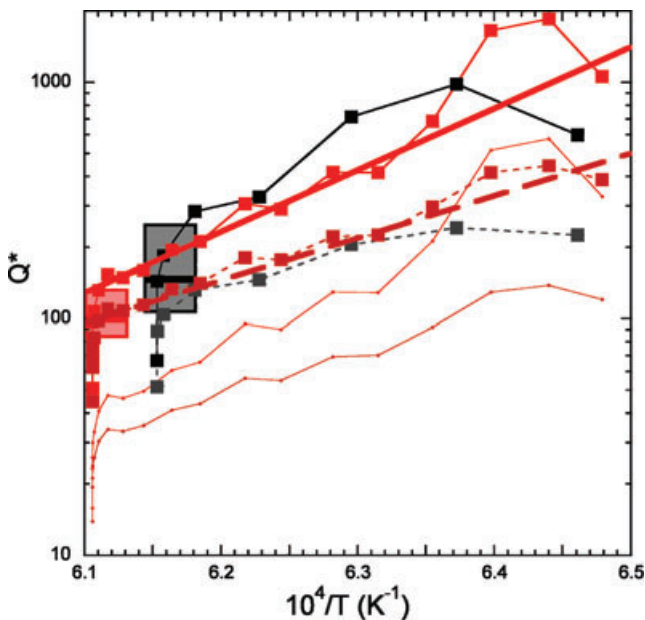


**Figure 6.** Apparent quality factor of shear waves in the lithospheric oceanic mantle from eq. (3) for a  $\alpha$  exponent of 0.1 (squares) and 0.3 (dots), using data from Priestley and McKenzie (2006). Red (75 km depth) and black (50 km depth) symbols with full lines for  $V_S$  models accounting for elastic softening of OPx, dark red (75 km depth) and grey (50 km depth) symbols and broken lines for  $V_S$  models with linear temperature dependence. Results for  $\alpha$  exponent of 0.3 are shifted from those for  $\alpha$  of 0.1 by a constant factor of about 3.2, and are shown only for 75 km depth. Thick lines show the Arrhenius fits over the whole plotted  $T$  range. Boxes show  $Q$  factor range (thick line is the average) at 25–60 km and 55–140 km (Yang *et al.*, 2007), in grey and red, respectively.

$Q^*$  estimates. Hence results for the largest interval are discussed. The activation energies depend on the thermal parameters of the cooling model and on the elastic model of  $V_S$ , but do not depend on  $\alpha$ . Higher activation energies are obtained for the thermal model used by Priestley & McKenzie (2006) than for the model of Jaupart *et al.* (2007), of about 450 and 350 kJ mol<sup>-1</sup>, respectively, for the linear elastic model (Stixrude & Lithgow-Bertelloni 2005a), and of 660 and 500 kJ mol<sup>-1</sup>, respectively, for the soft OPx elastic model. The values for the linear elastic model are consistent with the activation energy of 424 kJ mol<sup>-1</sup> for grain size dependent attenuation (Jackson *et al.* 2002), but  $\alpha = 0.26$  associated with this relaxation mechanisms yields lower  $Q$  than observed from local seismological studies (Yang *et al.* 2007). Dislocation-creep in wet olivine with  $E = 430$  kJ mol<sup>-1</sup> (Karato & Wu 1993) is unlikely because water was removed from the olivine during interaction with melt at MOR (Karato & Jung 1998). The higher values of  $E$  for the OPx softening model are more consistent with those in the 500–700 kJ mol<sup>-1</sup> for attenuation in melt-bearing peridotite (Faul *et al.* 2004) or of 540 kJ mol<sup>-1</sup> for dislocation-creep in dry olivine (Karato & Wu 1993). Thus determination of the nature of the likely attenuation mechanism in the upper mantle critically depends on elastic softening in OPx.

## ACKNOWLEDGMENTS

Pascal Richet and Estelle Rose provided the OEn and SC samples, respectively. Dan McKenzie for providing shear velocity data for the oceanic lithosphere. Yanick Ricard and Jean-Paul Montagner for thoughtful comments and corrections. The Institut National des Sciences de l'Univers supports the national Raman facility at ENS Lyon. Additional support was provided through an international exchange program between CNRS and UIUC. This work was partially supported by the National Science Foundation through grants EAR-0738871 (to JDB).

## REFERENCES

- Afonso, J.C., Fernandez, M., Ranalli, G., Griffin, W.L. & Connolly, J.A.D., 2008. Integrated geophysical-petrological modeling of the lithosphere and sublithospheric upper mantle: methodology and applications, *Geochem. Geophys. Geosyst.*, **9**, Q05008, doi:05010.01029/02007gc001834.
- Anastasiou, P. & Seifert, F., 1972. Solid solubility of Al<sub>2</sub>O<sub>3</sub> in enstatite at high temperatures and 1–5 kb water pressure, *Contrib. Mineral. Petrol.*, **34**, 272–287.
- Angel, R.J., Chopelas, A. & Ross, N.L., 1992. Stability of high-density clinostatite at upper-mantle pressures, *Nature*, **358**, 322–324.
- Atlas, L., 1952. The polymorphism of MgSiO<sub>3</sub> and solid-state equilibria in the system MgSiO<sub>3</sub>–CaMgSi<sub>2</sub>O<sub>6</sub>, *J. Geol.*, **60**, 125–147.
- Bass, J.D., 1989. Elasticity of grossular and spessartite garnets by Brillouin spectroscopy, *J. geophys. Res.*, **94**, 7621–7628.

- Boyd, F.R., England, J.L. & Davis, B.T.C., 1964. Effects of pressure on the melting and polymorphism of enstatite  $\text{MgSiO}_3$ , *J. geophys. Res.*, **69**, 2101–2109.
- Brown, W.L., Morimoto, N. & Smith, J.V., 1961. A structural explanation of the polymorphism and transitions of  $\text{MgSiO}_3$ , *J. Geol.*, **69**, 609–616.
- Carpenter, M.A. & Salje, E.K.H., 1998. Elastic anomalies in minerals due to structural phase transitions, *European J. Mineral.*, **10**, 693–812.
- Chen, C.H. & Presnall, D.C., 1975. The system  $\text{Mg}_2\text{SiO}_4$ - $\text{SiO}_2$  at pressures up to 25 kilobars, *Am. Mineral.*, **60**, 398–406.
- Faul, U.H., Gerald, J.D.F. & Jackson, I., 2004. Shear wave attenuation and dispersion in melt-bearing olivine polycrystals: 2. Microstructural interpretation and seismological implications, *J. geophys. Res.-Solid Earth*, **109**, B06202, doi:06210.01029/02003jb002407.
- Forsyth, D.W. *et al.*, 1998. Imaging the deep seismic structure beneath a mid-ocean ridge: the MELT experiment, *Science*, **280**, 1215–1218.
- Gatta, G.D., Rinaldi, R., Knight, K.S., Molin, G. & Artioli, G., 2007. High temperature structural and thermoelastic behaviour of mantle orthopyroxene: an in situ neutron powder diffraction study, *Phys. Chem. Mineral.*, **34**, 185–200.
- Jackson, I., Fitz Gerald, J.D., Faul, U.H. & Tan, B.H., 2002. Grain-size-sensitive seismic wave attenuation in polycrystalline olivine, *J. geophys. Res.-Solid Earth*, **107**, B12360, doi:12310.11029/12001jb001225.
- Jackson, J.M., Sinogeikin, S.V., Carpenter, M.A. & Bass, J.D., 2004a. Novel phase transition in orthoenstatite, *Am. Mineral.*, **89**, 239–245.
- Jackson, J.M., Sinogeikin, S.V., Carpenter, M.A. & Bass, J.D., 2004b. Erratum to “Novel phase transition in orthoenstatite”, *Am. Mineral.*, **89**, 663.
- Jaupart, C., Labrosse, S. & Mareschal, J.C., 2007. Temperatures, heat and energy in the mantle of the earth. in *Treatise on Geophysics*, pp. 253–303, ed. Schubert, G., Elsevier, Amsterdam.
- Karato, S. & Jung, H., 1998. Water, partial melting and the origin of the seismic low velocity and high attenuation zone in the upper mantle, *Earth planet. Sci. Lett.*, **157**, 193–207.
- Karato, S. & Wu, P., 1993. Rheology of the upper mantle—a synthesis, *Science*, **260**, 771–778.
- Kawakatsu, H., Kumar, P., Takei, Y., Shinohara, M., Kanazawa, T., Araki, E. & Suyehiro, K., 2009. Seismic evidence for sharp lithosphere-asthenosphere boundaries of oceanic plates, *Science*, **324**, 499–502.
- Kung, J., Li, B.S., Uchida, T., Wang, Y.B., Neuville, D. & Liebermann, R.C., 2004. In situ measurements of sound velocities and densities across the orthopyroxene  $\rightarrow$  high-pressure clinopyroxene transition in  $\text{MgSiO}_3$  at high pressure, *Phys. Earth planet. Inter.*, **147**, 27–44.
- Kushiro, I., Yoder, H.S. & Nishikawa, M., 1968. Effect of water on the melting of enstatite, *Geol. Soc. Am. Bull.*, **79**, 1685–1692.
- Lekic, V., Matas, J., Panning, M. & Romanowicz, B., 2009. Measurement and implications of frequency dependence of attenuation, *Earth planet. Sci. Lett.*, **282**, 285–293.
- Maggi, A., Debayle, E., Priestley, K. & Barruol, G., 2006a. Multimode surface waveform tomography of the Pacific Ocean: a closer look at the lithospheric cooling signature, *Geophys. J. Int.*, **166**, 1384–1397.
- Maggi, A., Debayle, E., Priestley, K. & Barruol, G., 2006b. Azimuthal anisotropy of the Pacific region, *Earth planet. Sci. Lett.*, **250**, 53–71.
- Minster, J.B. & Anderson, D.L., 1981. A model of dislocation-controlled rheology for the mantle, *Phil. Trans. R. Soc. Lond. Series A, Math. Phys. Eng. Sci.*, **299**, 319–356.
- Nettles, M. & Dziewonski, A.M., 2008. Radially anisotropic shear velocity structure of the upper mantle globally and beneath North America, *J. geophys. Res.-Solid Earth*, **113**, B02303, doi:02310.01029/02006jb004819.
- Nishimura, C.E. & Forsyth, D.W., 1989. The Anisotropic Structure of the Upper Mantle in the Pacific, *Geophys. J.-Oxf.*, **96**, 203–229.
- Ohi, S., Miyake, A., Shimobayashi, N., Yashima, M. & Kitamura, M., 2008. An isosymmetric phase transition of orthopyroxene found by high-temperature X-ray diffraction, *Am. Mineral.*, **93**, 1682–1685.
- Okuno, M., Reynard, B., Shimada, Y., Syono, Y. & Willaime, C., 1999. A Raman spectroscopic study of shock-wave densification of vitreous silica, *Phys. Chem. Minerals.*, **26**, 304–311.
- Pacalo, R.E.G. & Gasparik, T., 1990. Reversals of the orthoenstatite-clinoenstatite transition at high-pressures and high-temperatures, *J. geophys. Res.-Solid Earth Planets*, **95**, 15853–15858.
- Pine, A.S. & Tannenwald, P.E., 1969. Temperature dependence of Raman linewidth and shift in  $\alpha$ -quartz, *Phys. Rev.*, **178**, 1424–1430.
- Priestley, K. & McKenzie, D., 2006. The thermal structure of the lithosphere from shear wave velocities, *Earth planet. Sci. Lett.*, **244**, 285–301.
- Reynard, B., Bass, J.D. & Jackson, J.M., 2008. Rapid identification of steatite-enstatite polymorphs at various temperatures, *J. Eur. Ceram. Soc.*, **28**, 2459–2462.
- Ross, N.L. & Reynard, B., 1999. The P21/c to C2/c transition in (Mg, Fe) $\text{SiO}_3$  pyroxenes, *Eur. J. Mineral.*, **11**, 585–589.
- Rychert, C.A. & Shearer, P.M., 2009. A global view of the lithosphere-asthenosphere boundary, *Science*, **324**, 495–498.
- Sadanaga, R. & Okamura, F.P., 1969. X-ray study of phase transformations of enstatite, *Proc. Japan Acad.*, **45**, 721–726.
- Sharma, S.K., 1989. Applications of advanced Raman spectroscopic techniques in earth sciences. in *Raman Spectroscopy Sixty Years on Vibrational Spectra and Structure*, pp. 513–568, eds Bist, H., Durig, J. & Sullivan, J., Elsevier, Amsterdam.
- Shimobayashi, N. & Kitamura, M., 1991. Phase-transition in Ca-poor clinopyroxenes—a high-temperature transmission electron-microscopic study, *Phys. Chem. Minerals.*, **18**, 153–160.
- Sinogeikin, S.V., Jackson, J.M., O'Neill, B., Palko, J.W. & Bass, J.D., 2000. Compact high-temperature cell for Brillouin scattering measurements, *Rev. Sci. Instrum.*, **71**, 201–206.
- Smith, J.V., 1959. The crystal structure of proto-enstatite,  $\text{MgSiO}_3$ , *Acta Crystallographica*, **12**, 515–519.
- Smyth, J.R., 1971. Protoenstatite—crystal-structure refinement at 1100 degrees C, *Zeitschrift Fur Kristallographie Kristallgeometrie Kristallphysik Kristallchemie*, **134**, 262–274.
- Smyth, J.R., 1974. Experimental study on polymorphism of enstatite, *Am. Mineral.*, **59**, 345–352.
- Stixrude, L. & Lithgow-Bertelloni, C., 2005a. Mineralogy and elasticity of the oceanic upper mantle: origin of the low-velocity zone, *J. geophys. Res.-Solid Earth*, **110**, B03204, doi:03210.01029/02004jb002965.
- Stixrude, L. & Lithgow-Bertelloni, C., 2005b. Thermodynamics of mantle minerals—I. Physical properties, *Geophys. J. Int.*, **162**, 610–632.
- Sueno, S., Cameron, M. & Prewitt, C.T., 1976. Orthoferrosilite—high-temperature crystal-chemistry, *Am. Mineral.*, **61**, 38–53.
- Sueno, S., Kimata, M. & Prewitt, C.T., 1984. The crystal-structure of high-clinoferrosilite, *Am. Mineral.*, **69**, 264–269.
- Thieblot, L., Tequi, C. & Richet, P., 1999. High-temperature heat capacity of grossular ( $\text{Ca}_3\text{Al}_2\text{Si}_3\text{O}_{12}$ ), enstatite ( $\text{MgSiO}_3$ ), and titanite ( $\text{CaTiSiO}_5$ ), *Am. Mineral.*, **84**, 848–855.
- Weeraratne, D.S., Forsyth, D.W., Yang, Y.J. & Webb, S.C., 2007. Rayleigh wave tomography beneath intraplate volcanic ridges in the South Pacific, *J. geophys. Res.-Solid Earth*, **112**, B06303, doi:06310.01029/02006JB004403.
- Yang, H.X. & Ghose, S., 1995. A transitional structural state and anomalous Fe-Mg order-disorder in Mg-rich orthopyroxene, ( $\text{Mg}_{0.75}\text{Fe}_{0.25}$ ) $\text{Si}_2\text{O}_6$ , *Am. Mineral.*, **80**, 9–20.
- Yang, Y.J., Forsyth, D.W. & Weeraratne, D.S., 2007. Seismic attenuation near the East Pacific Rise and the origin of the low-velocity zone, *Earth planet. Sci. Lett.*, **258**, 260–268.
- Zucker, R. & Shim, S.H., 2009. In situ Raman spectroscopy of  $\text{MgSiO}_3$  enstatite up to 1550 K, *Am. Mineral.*, **94**, 1638–1646.

#### APPENDIX: CALCULATION OF $V_S$ OF ORTHOPYROXENE AT MANTLE PRESSURE AND TEMPERATURE

To extrapolate effects of the critical behaviour of  $V_S$  around  $T_C$  to upper mantle, we have to constrain the evolution of  $T_C$ ,  $n$  and  $V_S(T_r)$  with pressure and temperature. The Clapeyron slope  $\partial T_C / \partial P = 210 \pm 90 \text{ K GPa}^{-1}$  is estimated from phase equilibrium data (Fig. 3). Thus values of 100, 200 and 300  $\text{K.GPa}^{-1}$  were tested, assuming the

value of 1454 K for  $T_C$  in SC OPx at ambient pressure for mantle orthopyroxene. The temperature derivative of  $V_S$  is:

$$\left. \frac{\partial \ln V_S}{\partial T} \right)_P = -\frac{1}{n(P)T_C(P)} \left( 1 - \frac{T}{T_C(P)} \right)^{-1}, \quad (\text{A1})$$

that decreases by a factor of 3–7 between 0 and 10 GPa at  $T < 1200$  K when increasing  $T_C$  with pressure without changing the other parameters. This is unrealistic and incompatible with self-consistent thermodynamic modelling (Stixrude & Lithgow-Bertelloni 2005b) yielding a variation of  $\partial \ln V_S / \partial T$  from about  $10^{-4} \text{ K}^{-1}$  at ambient pressure to  $8 \times 10^{-5} \text{ K}^{-1}$  at 10 GPa. Forcing the product  $n(P)T_C(P)$  to vary less rapidly with pressure by varying  $n$  results in  $\partial \ln V_S / \partial T$  decreasing less rapidly with pressure. Thus we constrained the evolution of  $n$  with pressure in order to keep the temperature derivative of  $V_S$  consistent with the thermodynamic data set of Stixrude & Lithgow-Bertelloni (2005b). Noting that the sublinear decrease of  $V_S$  in their model corresponds roughly to the slope given by eq. (1) at 873 K (Fig. 1), we adjusted the evolution of  $n$  with pressure so that  $\partial \ln V_S / \partial T$  at 873 K varies from  $10^{-4} \text{ K}^{-1}$  at ambient pressure to  $8 \times 10^{-5} \text{ K}^{-1}$  at 10 GPa and find

$$n(P) = n_0 \left( \frac{T_C + 15P - 873}{T_C + \frac{dT_C}{dP}P - 873} \right). \quad (\text{A2})$$

$V_S(T_r, P) / V_S(T_r, 0)$  is conveniently calculated from the formalism and data set of Stixrude & Lithgow-Bertelloni (2005b). However starting from  $V_S(298, P)$  of Stixrude & Lithgow-Bertelloni (2005b) results in a difference with the present model that will increase from 0 at 298 K to reach a maximum near 873 K at ambient pressure (Fig. 1) because of the curvature in  $V_S$  (eq. 1). In order to minimize the difference between the two models in the 1200 K range where quasi-harmonic and anharmonic models should in average give comparable results, we have added a slight correction to the shear velocity at 298 K in our model using the expression:

$$\begin{aligned} V_{S\text{corrected}}(298, P) \\ = V_S(298, P) \left[ 1 - 0.01 \left( \frac{T_C - 873}{T_C + \frac{dT_C}{dP}P - 873} \right) \right] \end{aligned} \quad (\text{A3})$$

that yields satisfactory results (Fig. 4). Thus the present model gives a match to available shear velocity data over a wide range of pressure and temperature with five adjustable parameters ( $T_C$  at ambient pressure,  $n$  and  $V_S(298, 0)$  and their pressure derivative) and one variable,  $dT_C/dP$ , independently constrained from phase equilibrium data.